

# Full 3D+1 modelling of the tilted-pulse-front setups for single-cycle terahertz generation

Lu Wang<sup>1,2\*</sup>, Tobias Kroh<sup>1,2</sup>, Nicholas H. Matlis<sup>1</sup>, and Franz Kärtner<sup>1,2,3</sup>

\*lu.wang@desy.de

<sup>1</sup>Center for Free Electron Laser Science, Deutsches Elektronen-Synchrotron Notkestraße 85, 22607 Hamburg  
<sup>2</sup>Department of Physics, Universität of Hamburg, Luruper Chaussee 149, 22761 Hamburg, Germany  
<sup>3</sup>The Hamburg Centre for Ultrafast Imaging (CUI), Luruper Chaussee 149, 22761 Hamburg, Germany

April 23, 2022

## Abstract

The tilted-pulse-front setup utilizing a diffraction grating is one of the most successful methods to generate single- to few-cycle terahertz pulses. However, the generated terahertz pulses have a large spatial inhomogeneity, due to the noncollinear phase matching condition and the asymmetry of the prism-shaped nonlinear crystal geometry, especially when pushing for high optical-to-terahertz conversion efficiency. A 3D+1 (x,y,z,t) numerical model is necessary in order to fully investigate the terahertz generation problem in the tilted-pulse-front scheme. We compare in detail the differences between 1D+1, 2D+1 and 3D+1 models. The simulations show that the size of the optical beam in the pulse-front-tilt plane sensitively affects the spatio-temporal properties of the terahertz electric field. The terahertz electric field is found to have a strong spatial dependence such that a few-cycle pulse is only generated near the apex of the prism. The part of the beam farther from the apex contains a large fraction of the energy but has a waveform that deviates from a few-cycle. This strong spatial dependence must be accounted for when using the terahertz pulses for strong-field physics and carrier-envelope-phase sensitive experiments such as terahertz acceleration, coherent control of antiferromagnetic spin waves and terahertz high-harmonic generation.

# 1 Introduction

Single- to few-cycle (broadband) high energy terahertz pulses have many promising applications such as spectroscopy [6], strong field terahertz physics[14, 20], particle acceleration [25], electron spin manipulation [14] and phonon resonance studies [1]. All of these applications require well-characterized terahertz fields.

There are many possible ways to generate terahertz radiation. Free electron lasers and synchrotron radiation have a high degree of tunability and are capable of delivering high peak-power coherent terahertz pulses [22]. Gyrotrons, based on the principle of electron cyclotron radiation, are able to generate watt-to-megawatt-level terahertz continuous wave radiation [11] at low terahertz frequencies (0.3-1.3 THz)[5, 4]. These devices, however, have limited accessibility to the larger scientific community, and can be difficult to synchronize to laser sources with high (fs) precision.

Alternatively, single- to few-cycle terahertz generation, based on table-top optical laser systems, brings the advantages of high accessibility and intrinsic synchronization, but suffers from limited optical-to-terahertz conversion efficiency. Although various schemes exist for optical-to-terahertz conversion, difference frequency generation using the tilted pulse-front (TPF) method has proven one of the most useful. Using the "tilted-pulse-front" technique, first proposed and demonstrated by J.Hebling et.al.[12], pulse energies in the millijoule range can be reached[10]. The ease of this setup, the high pulse energies and the controllability of the terahertz properties has made this last approach an ubiquitous one for high-field applications.

However, the non-collinear geometry of the phase matching and the spatial asymmetry of the interaction, in combination with the cascading effect, result in terahertz beams with non-uniform spatial distribution. A 2D+1 numerical model has been established by M. I. Bakunov [2, 3] where the back conversion of the terahertz to the optical pump (OP) is not taken into consideration. Consequently, this model overestimates the effective length and the conversion efficiency. Later on, in our previous work the interaction between the optical pump and the terahertz pulse is included into the 2D+1 model together with a one lens imaging system by K. Ravi [17]. Compared with the telescope imaging system, the one-lens imaging system, has larger imaging errors and induces more terahertz divergence [23]. In order to further investigate the terahertz generation problem, a robust 3D+1 numerical tool is necessary to explore the spatial and temporal properties of the generated terahertz fields. In our work, a telescope imaging system is used. Additionally, the image of the grating is chosen to be parallel to the pulse-front-tilt plane inside the nonlinear crystal [8]. Thus, along the image plane at each spatial point, the OP forms transform limited pulse, i.e. the peak intensity is the maximum and the bandwidth is the maximum. This work shows, for the first time to our knowledge, the systematic comparison of the 1D+1, 2D+1 and 3D+1 numerical models. Additionally, it simulates precisely the full spatial distribution of the generated terahertz electric fields.

The numerical tool is based on the fast Fourier transform beam propagation

method (FFT-BPM) [7] and split-step Fourier method. The combination of these two methods reduces computational cost compared to the finite difference time-domain (FDTD) method which is very accurate but requires a massive computational effort. In section 2, we show analytically that the higher order dispersion caused by the grating can already bring in spatial inhomogeneity to the generated terahertz pulses. Section 3 compares the differences of the 1D+1, 2D+1 and 3D+1 models. In section 4, the dependence of optical pump beam sizes in  $y$  and  $x$  directions on the generated terahertz fields are discussed.

## 2 Theoretical model

The setup modelled and simulated is shown in Fig. 1. The often used nonlinear materials are LiNbO<sub>3</sub>, CdTe, GaAs, GaSe, GaP and ZnTe. Here, we focus on LiNbO<sub>3</sub> (LN for short) due to its large second-order nonlinear coefficient, high damage threshold and easy accessibility. The results however can be extended to other materials. In this article, we focus on the impact of the OP beam size on the properties of the generated terahertz beam.

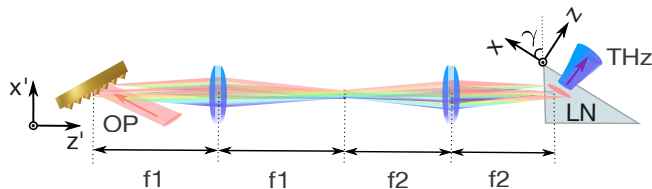


Figure 1: Illustration of the simulated tilted-pulse-front setup. The optical pump pulse is noted by OP and the LiNbO<sub>3</sub> crystal is represented by LN. The OP propagates along the  $z'$  direction. The  $x - y - z$  coordinates denote the pulse-front-tilt frame (terahertz frame) inside the LN-crystal. The  $y$  and  $y'$  axes are equivalent.

Firstly, we show analytically that, regardless of the noncollinear phase matching and the prism geometry, the second order dispersion generated by the grating can already cause inhomogeneity of the terahertz pulses (see Eq. (4)). We start from the grating relation  $\sin(\theta_1) + \sin(\theta_2) = 2\pi c/\omega d$ , where  $\theta_1, \theta_2$  are the incidence and output angles with respect to the normal to the grating surface respectively. The optical frequency is represented by  $\omega$  while  $d$  denotes the grating groove period. Assuming that the input OP is collimated ( $d\theta_1/d\omega = 0$ ), one can get Eq.(1).

$$\begin{cases} \frac{d\theta_2}{d\omega} = \frac{-2\pi c}{\omega^2 d \cos(\theta_2)} \\ \frac{d^2\theta_2}{d^2\omega} = \frac{4\pi c}{\omega^3 d \cos(\theta_2)} + \frac{2\pi c \sin(\theta_2)}{\omega^2 d \cos^2(\theta_2)} \frac{d\theta_2}{d\omega} \end{cases} \quad (1)$$

By setting  $F_0 = -2\pi c/(\omega_0^2 d \cos(\theta_2))$  where  $\omega_0$  is the center frequency, one can obtain the angular dispersion  $\Delta\theta_2$  with respect to the OP propagation direction,

$$\begin{aligned}\Delta\theta_2 &= \left. \frac{d\theta_2}{d\omega} \right|_{\omega=\omega_0} (\omega - \omega_0) + \frac{1}{2} \left. \frac{d^2\theta_2}{d^2\omega} \right|_{\omega=\omega_0} \Delta(\omega - \omega_0)^2 \\ &= F_0 (\omega - \omega_0) + \left[ -F_0/\omega_0 + \frac{1}{2} F_0^2 \tan(\theta_2) \right] (\omega - \omega_0)^2.\end{aligned}\quad (2)$$

The  $\cos(\theta_2), \tan(\theta_2)$  represent the cosine and tangent of the output angle at the center frequency  $\omega_0$ . After the propagation through the telescope system, the angular dispersion is magnified by a factor of  $-f_2/f_1$ . Thus, the angular dispersion becomes  $-\Delta\theta_2 f_2/f_1$ . Note that the transverse k vector  $k_{x'0}(\omega) = -\Delta\theta_2 f_2 \omega_0 / (c f_1)$  remains the same before and after entering the LN-crystal due to the Fresnel law. As a result, by assuming  $k_{z'0}(\omega) \approx \omega n(\omega)/c$ , the OP electric field inside the LN-crystal is given in Eq. (3) in the  $x' - y' - z'$  coordinates, where the pulse duration  $\tau = \tau_0/\sqrt{2 \log 2}$ , and  $\sigma'_x, \sigma'_y$  are beam waists (1/e) of the OP at the incidence surface of the LN-crystal in  $x'$  and  $y'$  dimensions respectively.

$$\begin{aligned}E(\omega, x', y', z') &= A_0 \exp [-(\omega - \omega_0)^2 \tau^2 / 4] \exp [-x'^2 / (2\sigma_x'^2)] \exp [-y'^2 / (2\sigma_y'^2)] \\ &\quad \times \exp [-i\omega n(\omega) z' / c] \exp [i\Delta\theta_2 f_2 \omega_0 x' / (c f_1)]\end{aligned}\quad (3)$$

The second order polarization which is responsible for the terahertz generation can be expressed as in Eq. (4), where  $\gamma$  is the angle between the terahertz pulse propagation direction and the OP propagation direction. The group refractive index at the center frequency of the optical pump is denoted by  $n_g$ .

$$\begin{aligned}P^{NL(2)}(\Omega, x', y', z') &= -\chi^{(2)} \frac{\Omega^2}{c^2} \int_0^\infty E(\omega + \Omega, x', y', z') E^*(\omega, x', y', z') d\omega \\ &\quad \times \exp \{i\Omega n(\Omega) [\cos(\gamma) z' + \sin(\gamma) x'] / c\} \\ &= -\chi^{(2)} \frac{\Omega^2 \sqrt{2\pi}}{\tau c^2} A_0^2 \exp \left( \frac{-x'^2}{\sigma_x'^2} \right) \exp \left( \frac{-y'^2}{\sigma_y'^2} \right) \\ &\quad \times \exp \left\{ -\frac{\Omega^2 \tau^2}{8} \left[ 1 + \frac{16x'^2 n_g^2 \tan(\gamma)^2}{\tau^4 c^2} (-1/\omega_0 + \frac{1}{2} F_0 \tan(\theta_2))^2 \right] \right\} \\ &\quad \times \exp \left\{ -i \frac{\Omega}{c} [n_g - n(\Omega) \cos(\gamma)] z' \right\} \exp \left\{ i \left[ \frac{f_2 \omega_0}{f_1} F_0 + n(\Omega) \sin(\gamma) \right] \frac{\Omega}{c} x' \right\}\end{aligned}\quad (4)$$

The last two exponential phase terms in Eq. (4) represent the phase match-

ing condition.

$$\begin{cases} \Delta k'_z = \frac{\Omega}{c} [n_g - n(\Omega) \cos(\gamma)] = 0 \rightarrow n_g/n(\Omega) = \cos(\gamma) \\ \Delta k'_x = \left[ \frac{f_2 \omega_0}{f_1} F_0 + n(\Omega) \sin(\gamma) \right] \frac{\Omega}{c} = 0 \rightarrow \frac{2\pi c f_2}{d \cos(\theta_2) \omega_0 n_g f_1} = \tan(\gamma) \end{cases}$$

The term in the third exponential ( $[-1/\omega_0 + \frac{1}{2}F_0 \tan(\theta_2)]^2 16x^2 n_g^2 \tan(\gamma)^2 / \tau^4 c^2$ ) is due to the second order angular dispersion which has been discussed in more detail in [18]. It can be seen that the second order angular dispersion leads to the spatial dependence of the generated terahertz bandwidth at the plane normal to the OP propagation direction. At the center of the pump pulse ( $x' = 0$ ), the generated terahertz pulse possesses its largest bandwidth. Towards the sides of the OP beam, the bandwidth of the terahertz pulse reduces. In other words, due to the second order angular dispersion ( $(\omega - \omega_0)^2$  related term), the OP experiences a temporal chirp and thus, the pulse duration varies with respect to  $x'$ . The effective instantaneous bandwidth of the OP reduces towards the sides of the beam, leading to a narrower terahertz spectrum or multi-cycle pulses.

### 3 Comparison of the 1D+1, 2D+1 and 3D+1 simulations

Owing to the geometry of the LN-crystal, the interaction length varies with respect to  $x'$ . Since the generated terahertz pulses act back on to the OP, cascading occurs. This causes a spatially dependent OP spectrum, which further enhances spatial inhomogeneities of the generated terahertz pulses. Furthermore, at the desired terahertz frequency range (<4 THz), the material absorption ( $\alpha$ ) increases with respect to frequency. This favors lower terahertz frequencies towards the base of the LN-crystal due to longer interaction length. The aforementioned aspects can only be investigated by a robust numerical model.

Our numerical model solves the coupled wave equations with slowly varying amplitude approximation in the terahertz coordinates (x-y-z). By setting the electric field of the OP  $\mathcal{F}[E_{\text{op}}(t, x, y, z)] = E_{\text{op}}(\omega, x, y, z) = E(\omega, x, y, z)e^{-i[k_{z0}(\omega)z + k_{x0}(\omega)x]}$ , and the electric field of the terahertz  $\mathcal{F}[E_{\text{THz}}(t, x, y, z)] = E_{\text{THz}}(\Omega, x, y, z) = E(\Omega, x, y, z)e^{-ik_0(\Omega)z}$  respectively, one can get Eqs. (5) and (6). The operator

$\mathcal{F}$  represents the Fourier transform.

$$\begin{aligned}
-2ik_0(\Omega) \frac{\partial E(\Omega, x, y, z)}{\partial z} &= - \underbrace{\left[ \frac{\partial^2}{\partial y^2} + \frac{\partial^2}{\partial x^2} \right]}_{\text{neglected by 1D+1}} \underbrace{-i\alpha k_0(\Omega)}_{\text{neglected by 2D+1}} E(\Omega, x, y, z) \\
&\quad - \frac{\Omega^2 \chi^{(2)}}{c^2} \int_0^\infty E(\omega + \Omega, x, y, z) E^*(\omega, x, y, z) e^{i(\Delta k_z z + \Delta k_x x)} d\omega \quad (5) \\
-2ik_{z0}(\omega) \frac{\partial E(\omega, x, y, z)}{\partial z} &= - \underbrace{\left[ \frac{\partial^2}{\partial y^2} + \frac{\partial^2}{\partial x^2} - 2ik_{x0}(\omega) \frac{\partial}{\partial x} \right]}_{\text{neglected by 1D+1}} \underbrace{E(\omega, x, y, z)}_{\text{neglected by 2D+1}} \\
-\varepsilon_0 n^2(\omega_0) \frac{\omega^2}{c} \mathcal{F} \left\{ E_{\text{op}}(t, x, y, z) \int_{-\infty}^\infty n_2(\tau) E_{\text{op}}^2(t - \tau, x, y, z) d\tau \right\} &e^{i[k_{z0}(\omega)z + k_{x0}(\omega)x]} \\
&\quad - \frac{\omega^2 \chi^{(2)}}{c^2} \int_{-\infty}^\infty E(\omega + \Omega, x, y, z) E^*(\Omega, x, y, z) e^{i(\Delta k_z z + \Delta k_x x)} d\Omega \quad (6)
\end{aligned}$$

In Eqs. (5) and (6),  $\Delta k_x = k_{x0}(\omega) - k_{x0}(\omega + \Omega)$ ,  $\Delta k_z = k_{z0}(\omega) - k_{z0}(\omega + \Omega) + k_0(\Omega)$ . The  $\chi^{(2)}$  related terms are responsible for the second order non-linear effects, i.e., the terahertz generation and back conversion processes. In Eq. (6), the third-order nonlinear effects, including self-phase-modulation, self-steepening and stimulated Raman effect, are represented by the term  $n_2(\tau) = \mathcal{F}[n_2(\omega - \omega_0)]$  [13]. The phonon resonances at terahertz frequencies [21] are implemented by considering the stimulated Raman effect at the optical frequency region together with the frequency-dependent refractive index in the terahertz frequency region. In the simulation, frequency dependent refractive index and the terahertz absorption are used. The parameters used in simulations are listed in Table.1. The peak fluence of the OP at the input LN-crystal surface is chosen to be right beneath the estimated damage threshold  $70.7 \text{ mJ/cm}^2$  based on our previous studies[19].

Table 1: Simulation parameters

Parameters	Value	Parameters	Value
focal length $f_1$	300 mm	focal length $f_2$ [23]	$0.613 \times f_1$ mm
wavelength $\lambda$	1030 nm	grating period d	1/1500 mm
pulse duration $\tau_0$ (FWHM) [9]	0.5 ps	peak fluence[19]	$10^8 \sqrt{\tau_0}$ mJ/cm <sup>2</sup>
phase-matching frequency	0.3 THz	absorption coefficient $\alpha$ (300 k, 0.3 THz) [24]	7/cm

The 1D+1 calculation neglects diffraction effects and, more importantly, the spatial walk-off between the terahertz and OP beams. The neglected terms are marked in Eq. (5) and (6) by "neglected by 1D+1". The 2D+1 calculation neglects the diffraction in the dimension vertical to the pulse front tilt plane ( $y$ ), which is labeled by "neglected by 2D+1". In other words, the 1D+1 calculation considers a single spatial point at the location of the peak fluence of the OP, and the 2D+1 calculation considers one slice of the spatial points along the  $x$  dimension at  $y = 0$ , i.e., the center of the OP. As shown in Fig. 2, the 1D+1 calculation significantly overestimates the conversion efficiency and the OP spectrum broadening. Without taking the spatial walk-off (the operator  $2ik_{x0}\frac{\partial}{\partial x}$ ) into consideration, the 1D+1 calculation overestimates the OP spectral broadening, leading to a more pronounced stimulated Raman effect. The overestimated OP spectral broadening leads to the second peak in the terahertz spectrum at higher terahertz frequencies in Fig. 2(b).

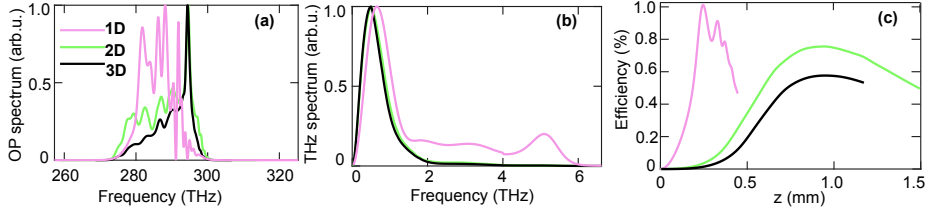


Figure 2: Comparison of the results obtained from 1D+1, 2D+1 and 3D+1 simulations. (a), (b) and (c) are the output OP spectra, the output terahertz spectra and the efficiencies respectively. (a) and (b) are plotted at the location of maximum efficiency.

In Fig. 2(c), from 1D to 2D, the decrease of efficiency is due to the longer interaction length, whereas from 2D to 3D the decrease of efficiency is due to the reduction of the fluence along the  $y$  direction. It can be seen that, in order to capture the key characteristics of the generated terahertz pulses, at least a 2D+1 calculation is required.

## 4 Spatial dependence of the terahertz electric field

Without loss of generality, the nonlinear interaction between the OP and the LN-crystal is numerically implemented in the  $x - y - z$  coordinate frame where  $x = 0$  represents the apex location of the LN-crystal. Note that the OP beam size in the  $x - y - z$  coordinates  $\sigma_x = \sigma_{x'} / \cos(\gamma)$  is due to the projection on the plane of the tilted pulse front. The simulations suggest that within an OP beam size range  $\sigma_y = [0.5, 4.5]$  mm (not shown), diffraction has a negligible effect on the terahertz generation process and the terahertz beam size scales as  $\sigma_y / \sqrt{2}$ . This agrees with the analytic result in Eq. (4). In the following simulations,  $\sigma_y$  is chosen to be 3.5 mm.

In Fig. 3, the maximum terahertz generation efficiency is plotted against the OP beam size  $\sigma_{x'}$ . Here, the 2D+1 model is used due to the high computational cost of the 3D+1 model. Generally, in the experiment, larger OP beam sizes and high fluence are desired due to the demand of high terahertz energy. As a result, in the following 3D+1 calculations for,  $\sigma_{x'} = 0.44\text{mm}$ ,  $0.88\text{mm}$  and  $1.32\text{mm}$ , indicated by red circles in Fig. 3, are chosen as examples.

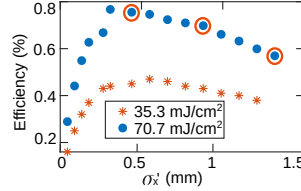


Figure 3: With the input pump fluence  $70.7\text{ mJ/cm}^2$  (blue dot) and  $35.3\text{ mJ/cm}^2$  (red star), the maximum terahertz generation efficiencies versus the OP beam size  $\sigma_{x'}$ , calculated by the 2D model, are presented. The red circles indicate 3 beam sizes chosen as examples in the following 3D+1 calculations.

Due to the nature of the non-collinear phase-matching condition, the terahertz generation process requires different sections of the beam along  $x$  dimension to add up coherently in the emission direction  $z$ . In contrast with the OP beam size in the  $y$  dimension, a small beam size along the  $x$  dimension cannot produce high generation efficiencies due to the walk-off between the OP and the terahertz beam. On the other hand, if the beam size is too large, the terahertz radiation generated by the wing of the OP at the farther side from the LN-crystal apex suffers from more absorption compared to the part closer to the apex. Thus, the generation efficiency shows a maximum as a function of OP beam size in the  $x'$ -direction. Additionally, since lower pump fluence leads to longer interaction length, the optimal pump beam size increases (see the red stars in Fig. 3).

Figure 4(j-l) indicate that with a given OP beam size, higher pump fluence (center of the OP,  $y = 0$ ) leads to smaller terahertz beam size compared with lower pump fluence (side of the OP  $y = \sigma_y/\sqrt{2} = 2.47\text{ mm}$ ). This agrees with the experimental results of C.Lombosi et al. [15].

Figure 4(a-c) and 4(d-f) show the OP and the terahertz beam profiles at the output LN-crystal surface with different input OP beam sizes. Note that the optimal interaction lengths along the  $z$  dimension increase with the increase of the OP beam sizes. For the beam sizes  $\sigma_x' = 0.44\text{ mm}$ ,  $0.88\text{ mm}$  and  $1.32\text{ mm}$ , the effective lengths are  $0.90\text{ mm}$ ,  $1.61\text{ mm}$  and  $2.12\text{ mm}$  with the corresponding conversion efficiencies  $0.57\%$ ,  $0.54\%$ ,  $0.46\%$  respectively. Figure 4(g-i) represent the fluence of the OP at  $y = 0$  and  $y = \sigma_y/\sqrt{2}$  with the center of the OP marked by the dashed lines. The fluence distribution indicates an energy shift towards the base of the LN-crystal, due to the terahertz generation process. In other words, terahertz generation process causes spectral broadening of the OP,



with which the non-collinear phase matching generates new optical frequencies propagating towards the base of the LN-crystal. This causes the energy shift in the OP fluence distribution. One can see that the terahertz beams are generated close to the apex of the LN-crystal. The size of the OP does not strongly influence the size of the generated terahertz beams. More detailed analyses show the spatially dependent electric field and spectra at two positions ( $y = 0$ ,  $y = \sigma_y/\sqrt{2}$ ) as presented in Fig. 5. The terahertz beams are symmetric along the  $y$  dimension.

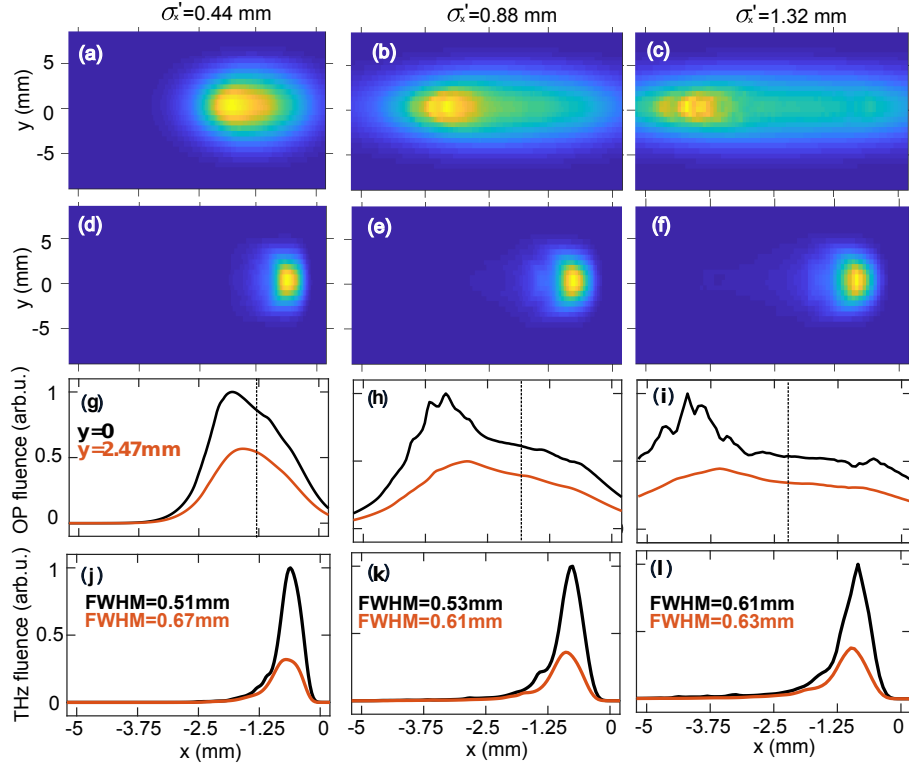


Figure 4: Spatial dependence of the generated terahertz beams along  $x$  and  $y$  dimensions. (a-c) and (d-f) represent the OP and the terahertz beam profiles at the output surface of the LN-crystal respectively. (g-i) and (j-l) represent the OP and terahertz fluence respectively at a given position  $y = 0$  (black curve) and  $y = \sigma_y/\sqrt{2} = 2.47$  (red curve). The OP beam sizes at the input LN-crystal surface are  $\sigma'_x = 0.44$  mm, 0.88 mm and 1.32 mm in  $x' - y' - z'$  frame respectively. The center position of the OP beam is marked by the dashed line. The OP beam size in the  $y$  dimension is  $\sigma_y = 3.5$  mm. The apex of the LN-crystal is located at  $x = 0$ .

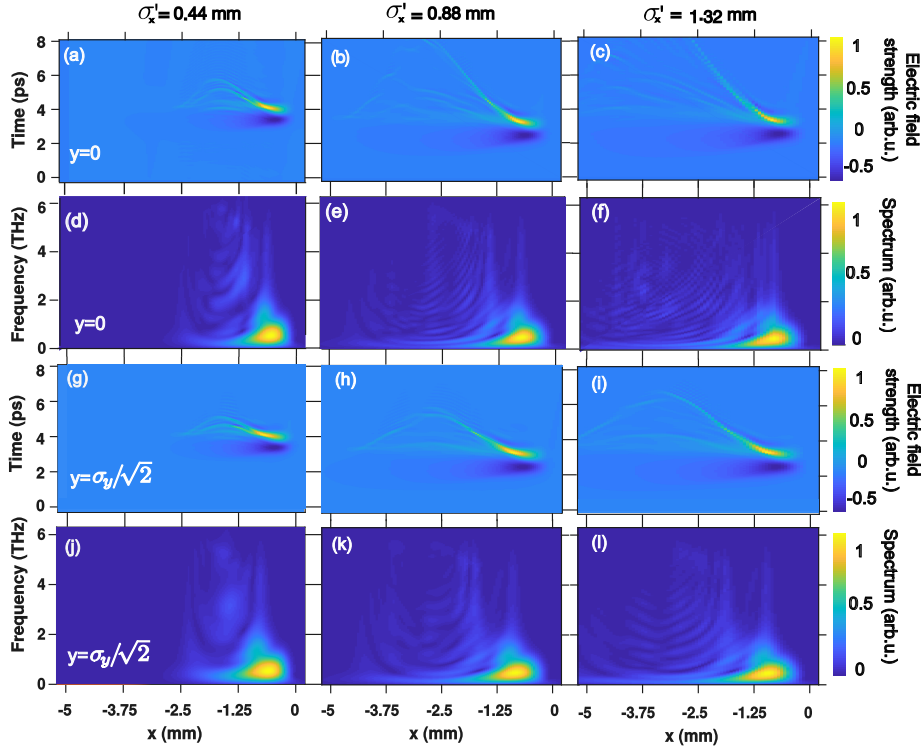


Figure 5: Spatial dependence of the generated terahertz spectra and temporal profiles along the  $x$  dimension. (a-c) and (d-f) are the terahertz electric field and the corresponding terahertz spectra with respect to  $x$  at  $y = 0$ . (g-i) and (j-l) are the terahertz electric field and the corresponding terahertz spectra with respect to  $x$  at  $y = \sigma_y/\sqrt{2}$ .

Figure 5 (a-c) and (g-i) show the spatially dependent electric fields at  $y = \sigma_y/\sqrt{2}$  and  $y = 0$  with the corresponding terahertz spectra shown in (d-f) and (j-l). It can be seen that the few-cycle terahertz electric fields are only generated at the vicinity of the apex of the LN-crystal. One can see that, for a terahertz beam generated by a large size OP, though possess a large amount of energy, the electric field at the far side from the apex of the LN-crystal deviates from a single-cycle format.

The root-mean-square pulse duration  $\Delta t$  is chosen to evaluate the electric field distribution. In Eq. (7),  $\delta t = |t(x, y) - t(x, y)_p|$ , where  $t(x, y)_p$  is the time coordinate of the peak of the electric field at position  $(x, y)$ . The reference  $\Delta t(x_p, y_p)$  is chosen at the position  $(x_p, y_p)$  where the terahertz peak fluence is located.

$$\Delta t(x, y) = \sqrt{\frac{\int [\delta t(x, y)]^2 I(t, x, y) dt}{\int I(t, x, y) dt} - \left[ \frac{\int \delta t(x, y) I(t, x, y) dt}{\int I(t, x, y) dt} \right]^2} \quad (7)$$

The resulting electric field distribution is depicted in Fig. 6. The shaded grey region represents  $\Delta t(x, y) > 2\Delta t(x_p, y_p)$ , which indicates that the electric field deviates from the single-cycle format.

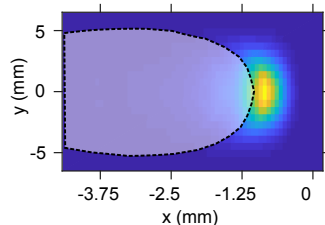


Figure 6: The example shown is for  $\sigma'_x = 1.32$  mm, where the non-single-cycle region,  $\Delta t(x, y) > 2\Delta t(x_p, y_p)$ , is indicated by the grey region. The terahertz beam under the grey region contains up to 25% of the total terahertz energy.

The grey region in Fig. 6 shows that high quality few-cycle pulses are only generated close to the apex of the LN-crystal. The terahertz pulses are symmetric along the  $y$ -direction. Higher fluence ( $y=0$ ) leads to higher terahertz energy but it also reduces the electric field quality i.e. less clean spectrum and multi-cycle format in time domain. It can be seen from Fig. 5 and Fig. 6 that the sides of the OP beam (for example  $y = \sigma_y/\sqrt{2}$  mm) possess lower fluence, causing less OP spectral broadening. The less broadened OP spectrum leads to a relatively homogeneous terahertz distribution along the  $x$  dimension. For  $\sigma_{x'} = 0.44$  mm,  $0.88$  mm and  $1.32$  mm the  $\Delta t(x, y) > 2\Delta t(x_p, y_p)$  region (grey region) take up 4%, 20% and 25% of the total terahertz energy respectively. It can be seen that, with the increase of the OP beam size, the single-cycle region of the generated terahertz pulses reduce drastically. Additionally, due to the nature of the setup itself, it is inevitable that the generated terahertz possesses a spatial inhomogeneity. In order to resolve this problem, the setup which combines the conventional tilted-pulse-front setup and a transmission stair-step echelon is promising in generating spatially homogeneous terahertz pulses [16].

## 5 Conclusion

We have shown the spatial dependence of the terahertz electric field properties generated by the tilted-pulse-front setup. By comparing the 1D+1, 2D+1 and 3D+1 numerical models we found that the 1D+1 calculation cannot capture certain key features of the terahertz generation process. Additionally, the 3D+1 calculation shows that within the OP beam size range  $\sigma_y = [0.5, 4.5]$  mm, the diffraction in the dimension perpendicular to the pulse-front-tilt plane does not have much influence on the terahertz generation process. For those cases, the 2D calculation ( $x$ - $z$  coordinates) is a good approximation.

Perpendicular to the pulse front tilt plane, in  $y$ -direction, the terahertz beam waist relates to the OP waist with  $\sigma_y/\sqrt{2}$ , which is as expected due to the second

order nonlinear process. In the  $x$  dimension, the OP beam size does not have a large impact on the generated terahertz beam size. The terahertz pulses are generated close to the apex of the LN-crystal and the single-cycle region is only close to the vicinity of the crystal apex. Thereby, large OP beam sizes lead to a reduced percentage of single-cycle content of the generated terahertz pulses. Attention must be paid to the fact that the terahertz generated farther from the apex of the LN-crystal, which possesses a large fraction of the total generated energy, suffers from poor electric field quality and temporal chirp.

These findings are of particular relevance to the carrier-envelope-phase sensitive terahertz applications and strong field terahertz physics. In order to maximize the single-cycle region, one should enlarge the OP beam size in the dimension vertical to the pulse-front-tilt plane ( $y$  dimension), or reduce the OP input fluence.

The terahertz out-coupling from the LN-crystal to the air is not considered in this article. This can further influence the terahertz output spectrum due to total internal reflection.

## Funding

European Union's Seventh Framework Program (FP7/2007-2013) through the Synergy Grant AXSIS (609920); The Hamburg Center for Ultrafast Imaging –Structure, Dynamics and Control of Matter at the Atomic Scale (CUI, DFG-EXC1074).

## Acknowledgment

We thank the DESY HPC team for providing access and computation time on the DESY Maxwell cluster. Lu Wang would like to thank IMPRS (International Max Planck Research School for Ultrafast Imaging & Structural Dynamics).

## References

- [1] HJ Bakker, S Hunsche, and H Kurz. Observation of thz phonon-polariton beats in LiTaO<sub>3</sub>. *Physical review letters*, 69(19):2823, 1992.
- [2] MI Bakunov, SB Bodrov, and MV Tsarev. Terahertz emission from a laser pulse with tilted front: Phase-matching versus cherenkov effect. *Journal of Applied Physics*, 104(7):073105, 2008.
- [3] Michael I Bakunov, Sergey B Bodrov, and Eugene A Mashkovich. Terahertz generation with tilted-front laser pulses: dynamic theory for low-absorbing crystals. *JOSA B*, 28(7):1724–1734, 2011.
- [4] VL Bratman, AA Bogdashov, GG Denisov, M Yu Glyavin, Yu K Kalynov, AG Luchinin, VN Manuilov, VE Zapevalov, NA Zavolsky, and VG Zorin.

- Gyrotron development for high power thz technologies at iap ras. *Journal of Infrared, Millimeter, and Terahertz Waves*, 33(7):715–723, 2012.
- [5] VL Bratman, Yu K Kalynov, and VN Manuilov. Large-orbit gyrotron operation in the terahertz frequency range. *Physical review letters*, 102(24):245101, 2009.
- [6] AG Davies, Edmund H Linfield, and Michael B Johnston. The development of terahertz sources and their applications. *Physics in Medicine & Biology*, 47(21):3679, 2002.
- [7] MD Feit and JA Fleck. Light propagation in graded-index optical fibers. *Applied optics*, 17(24):3990–3998, 1978.
- [8] JA Fülöp, L Pálfalvi, G Almási, and J Hebling. Design of high-energy terahertz sources based on optical rectification. *Optics express*, 18(12):12311–12327, 2010.
- [9] JA Fülöp, L Pálfalvi, S Klingebiel, G Almási, F Krausz, S Karsch, and J Hebling. Generation of sub-mj terahertz pulses by optical rectification. *Optics letters*, 37(4):557–559, 2012.
- [10] József A Fülöp, Zoltán Ollmann, Cs Lombosi, Christoph Skrobol, Sandro Klingebiel, László Pálfalvi, Ferenc Krausz, Stefan Karsch, and János Hebling. Efficient generation of thz pulses with 0.4 mj energy. *Optics express*, 22(17):20155–20163, 2014.
- [11] M Yu Glyavin, A Gu Luchinin, and G Yu Golubiatnikov. Generation of 1.5-kw, 1-thz coherent radiation from a gyrotron with a pulsed magnetic field. *Physical review letters*, 100(1):015101, 2008.
- [12] Janos Hebling, Gabor Almasi, Ida Z Kozma, and Jürgen Kuhl. Velocity matching by pulse front tilting for large-area thz-pulse generation. *Optics Express*, 10(21):1161–1166, 2002.
- [13] RW Hellwarth. Third-order optical susceptibilities of liquids and solids. *Progress in Quantum Electronics*, 5:1–68, 1977.
- [14] Tobias Kampfrath, Alexander Sell, Gregor Klatt, Alexej Pashkin, Sebastian Mährlein, Thomas Dekorsy, Martin Wolf, Manfred Fiebig, Alfred Leitenstorfer, and Rupert Huber. Coherent terahertz control of antiferromagnetic spin waves. *Nature Photonics*, 5(1):31, 2011.
- [15] Cs Lombosi, Gy Polónyi, Mátyás Mechler, Zoltán Ollmann, János Hebling, and JA Fülöp. Nonlinear distortion of intense thz beams. *New Journal of Physics*, 17(8):083041, 2015.
- [16] László Pálfalvi, György Tóth, Levente Tokodi, Zsuzsanna Márton, József András Fülöp, Gábor Almási, and János Hebling. Numerical investigation of a scalable setup for efficient terahertz generation using a segmented tilted-pulse-front excitation. *Optics express*, 25(24):29560–29573, 2017.

- [17] Koustuban Ravi, Wenqian Ronny Huang, Sergio Carbajo, Emilio A Nanni, Damian N Schimpf, Erich P Ippen, and Franz X Kärtner. Theory of terahertz generation by optical rectification using tilted-pulse-fronts. *Optics express*, 23(4):5253–5276, 2015.
- [18] Koustuban Ravi and Franz Kärtner. Analysis of terahertz generation using tilted pulse fronts. *Optics express*, 27(3):3496–3517, 2019.
- [19] Koustuban Ravi, Damian N Schimpf, and Franz X Kärtner. Pulse sequences for efficient multi-cycle terahertz generation in periodically poled lithium niobate. *Optics express*, 24(22):25582–25607, 2016.
- [20] Olaf Schubert, Matthias Hohenleutner, Fabian Langer, Benedikt Urbanek, C Lange, U Huttner, D Golde, T Meier, M Kira, Stephan W Koch, et al. Sub-cycle control of terahertz high-harmonic generation by dynamical bloch oscillations. *Nature Photonics*, 8(2):119, 2014.
- [21] Stanley Saul Sussman. Tunable light scattering from transverse optical modes in lithium niobate. Technical report, STANFORD UNIV CA MICROWAVE LAB, 1970.
- [22] Ping Tan, Jiang Huang, KaiFeng Liu, YongQian Xiong, and MingWu Fan. Terahertz radiation sources based on free electron lasers and their applications. *Science China Information Sciences*, 55(1):1–15, 2012.
- [23] Levente Tokodi, J Hebling, and L Pálfalvi. Optimization of the tilted-pulse-front terahertz excitation setup containing telescope. *Journal of Infrared, Millimeter, and Terahertz Waves*, 38(1):22–32, 2017.
- [24] Márta Unferdorben, Zsuzsanna Szaller, Ivett Hajdara, János Hebling, and László Pálfalvi. Measurement of refractive index and absorption coefficient of congruent and stoichiometric lithium niobate in the terahertz range. *Journal of Infrared, Millimeter, and Terahertz Waves*, 36(12):1203–1209, 2015.
- [25] Dongfang Zhang, Arya Fallahi, Michael Hemmer, Xiaojun Wu, Moein Fakhari, Yi Hua, Huseyin Cankaya, Anne-Laure Calendron, Luis E Zapata, Nicholas H Matlis, et al. Segmented terahertz electron accelerator and manipulator (steam). *Nature photonics*, page 1, 2018.